DALTON
FULL PAPER

Electron transfer in a trinuclear oxo-centred mixed-valence iron complex, in solid and solution states †

Christian Stadler,*‡[a] Jörg Daub,*[a] Jürgen Köhler,[b] Rolf W. Saalfrank,*[b] Veaceslav Coropceanu,[c] Volker Schünemann,[c] Claudia Ober,[c] Alfred X. Trautwein,*[c] Stewart F. Parker,[d] Mehmet Poyraz,[e] Tomohiko Inomata[e] and Roderick D. Cannon*[e]

[a] *Institut für Organische Chemie der Universität Regensburg, Universitätsstraße 31, D-93053 Regensburg, Germany*
[b] *Institut für Organische Chemie der Universität Erlangen-Nürnberg, Henkestraße 42, D-91054 Erlangen, Germany*
[c] *Institut für Physik der Medizinischen Universität Lübeck, Ratzeburger Allee 160, D-23538 Lübeck, Germany*
[d] *Rutherford Appleton Laboratory, Chilton, Didcot, UK OX11 0QX*
[e] *School of Chemical Sciences, University of East Anglia, Norwich, UK NR4 7TJ. E-mail: r.cannon@uea.ac.uk*

Received 23rd January 2001, Accepted 28th August 2001
First published as an Advance Article on the web 31st October 2001

Complexes $[Fe^{III}_2M^{II}OL_3]$ (M = Fe, Co, Ni, Cu; **2**, **3**, **4**, **5**) have been synthesised in which L^{2-} is a pentadentate ligand designed to coordinate all three metal atoms in the central cluster and to inhibit dissociation and solvent exchange processes. Crystal structures for **2**, **4** and **5** show threefold symmetry, attributed to rotational disorder. Magnetisation data for **2** indicate strong superexchange between basis oxidation states Fe(3+, 3+, 2+). Comparisons of IR spectra across the series of complexes confirm the non-threefold symmetry of the mixed-valence cluster on the vibrational time scale, both in the solid state and in solution. Proton NMR spectra in solution at room temperature do not distinguish the three iron sites, suggesting that pseudo-rotation by thermal electron transfer also operates. Cyclic voltammetry and spectroelectrochemical measurements show that the mixed-valence iron complex **2** can be oxidised reversibly to give the tri-iron(III) complex $[Fe_3OL_3]^+$ and reduced reversibly and quasireversibly to give respectively $[Fe_3OL_3]^-$ and tri-iron(II) $[Fe_3OL_3]^{2-}$, $E^0 = 85$, -635, -1230 mV (*versus* $Fc^{+/0}$) in dichloromethane ($T = 298$ K, 0.1 M $[n\text{-}Bu_4N][PF_6]$). Mössbauer spectra of **2** indicate significant valence delocalisation even at low temperature (4.2 K) with estimated valences Fe(2.9+, 2.9+, 2.2+) in the solid state. At higher temperatures no lifetime broadening is observed but additional Mössbauer absorptions are consistent with increasing proportions of trimer molecules with greater delocalisation, *i.e.* Fe(2.75+, 2.75+, 2.5+). In frozen solution (THF) the spectra indicate increasing proportions of molecules fully valence-delocalised on the Mössbauer time scale. The data are accounted for with a model which places the complex at the Robin–Day class III/II borderline. It combines strong superexchange with significant double exchange even at the lowest temperatures, while at higher temperatures in solution complete valence delocalisation occurs through intramolecular electron transfer at rates intermediate between the IR and NMR time scales.

Introduction

Electron transfer (ET) processes continue to be at the forefront of kinetic and mechanistic studies, with applications to fundamental processes in chemistry, physics and biology.[1] Especially valuable are model systems in which the electron moves between chemically equivalent sites where it is only weakly trapped, *i.e.* mixed-valence molecules at the borderline between localisation and delocalisation. Two-site exchange has been studied intensively,[2] and recent work has confirmed the role of solvent organisation, framework vibrations and magnetic exchange in controlling electron transfer rates.[3] Three-site exchange offers further possibilities. With suitable ligands, a wide variety of metal combinations can be assembled in a common framework; also the interactions can be studied through their direct effect on the molecular symmetry. One such class of compounds[4] has the central trimetallic unit bridged by carboxylate ligands, $[M_3O(OOCR)_6L_3]$, and is structurally related to the active sites of numerous iron–oxo proteins.[5] In this class, the transition between valence-localised and delocalised phases has been studied by crystallographic, thermodynamic and spectroscopic methods.[6] The dynamics of electron transfer and of coupled molecular motions have been measured in the solid state by NMR,[7] neutron scattering,[8] and infrared[9] spectroscopies. Solution studies however are complicated by rapid ligand-exchange reactions[10] and low stability of the reduced forms.[11] We have now been able to circumvent these limitations using the novel system $[M_3OL_3]$ (Scheme 1) in which

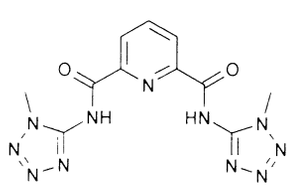

1: H_2L

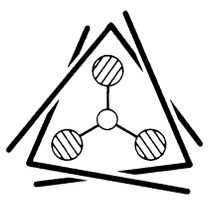

2-5: $[Fe_2MOL_3]$

Scheme 1

† Dedicated to Professor Dieter Sellmann on the occasion of his 60th birthday.
‡ Present address: Instituto de Catálisis y Petroleoquímica (CSIC), Campus Universidad Autónoma, Cantoblanco, 28049, Madrid, Spain.

DOI: 10.1039/b100780g

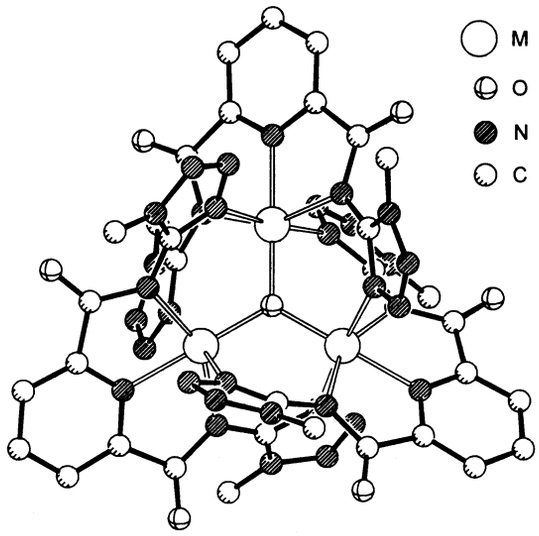

Fig. 1 Molecular structure of complexes $[Fe_3OL_3]^{n+}$ and $[Fe_2MOL_3]$.

each pentadentate ligand L simultaneously binds all three metal atoms. The molecular structure is shown in Fig. 1. As we show here, the complexes are robust in solution, and in case of the homonuclear complex $[Fe_3OL_3]$, **2**, all four redox states from $[M^{III}{}_3OL_3]^+$ to $[M^{II}{}_3OL_3]^{2-}$ are electrochemically accessible and can be characterised spectroscopically. The focus of this paper is the localisation or delocalisation of the 'extra' electron in the nominally mixed-valence cluster iron(III,III,II). It is perhaps worth stating that from our point of view, delocalisation can mean either of two things: mixing of wavefunctions so that the electronic configuration provides electron density distributed over more than one centre, or reversible variation of bond lengths so the electron in effect hops between centres at a definite frequency. We call these 'static' and 'dynamic' delocalisation, respectively. In a preliminary study[12] of **2**, Mössbauer spectra indicated that the iron valencies are localised, at least at 4.2 K, whereas the electrochemical data at first sight suggested delocalisation. Meanwhile, temperature-dependent Mössbauer spectra have been analysed[13] to show the existence of partially delocalised states in the solid state throughout the whole temperature range. To provide further insight into the electronic structure of this system we have now performed a range of further measurements, crystallographic, spectroscopic, electrochemical, and spectroelectrochemical, and we have compared the mixed-valence cluster with the oxidised tri-iron(III) and analogous mixed-metal complexes. We also outline a theoretical model consistent with the data and show finally that the mixed-valence molecule $[Fe_3OL_3]$, **2**, is close to the localised–delocalised limit, and very different from the analogous basic carboxylato-complexes.

Experimental

Materials

All reagents and solvents were purchased from commercial sources and used as received.

Synthesis

1-Methyl-5-aminotetrazole.[14] Methyl iodide (0.1 mol, 14.2 g) in 160 ml of acetone was added to a solution of 5-aminotetrazole monohydrate (0.1 mol, 10.3 g) and sodium hydroxide (0.1 mol, 4.0 g) in 40 ml of water. The mixture was heated for 3 h under reflux, evaporated to dryness and the residue extracted with five 50 ml portions of hot toluene. The toluene-insoluble material was dissolved in 25 ml of hot water and cooled at 5 °C. The solid material was removed by filtration, washed with 2 ml of cold water and crystallised from water. Yield 3.27 g (33%); mp 226 °C; ^{1}H NMR ([D$_6$]-DMSO, 400 MHz) δ 3.71 (s, 3 H, CH_3), 6.66 (s, 2 H, NH_2); ^{13}C NMR ([D$_6$]-DMSO, 100.5 MHz) δ 31.50 (CH_3), 155.84 (C=N); EI-MS *m*/*z* 99 (20%) $[C_2N_5H_5^+]$.

1-Trideuteromethyl-5-aminotetrazole. Prepared as above using trideuteromethyl iodide (0.1 mol, 14.5 g). Yield 3.47 g (34%); mp 207 °C; ^{1}H NMR ([D$_6$]-DMSO, 400 MHz) δ 6.63 (s, 2 H, NH_2); ^{13}C NMR ([D$_6$]-DMSO, 100.5 MHz) δ 30.86 (CD_3), 155.84 (C=N); EI-MS *m*/*z* 102 (100%) $[C_2N_5H_2D_3^+]$.

H_2L, 1.[15] A solution of 1-methyl-5-aminotetrazole (20 mmol, 1.98 g) in 25 ml of 1-methylpyrrolidin-2-one containing lithium chloride (2.0 g) was cooled to 0 °C, and 2,6-dichloroformyl pyridine (10 mmol, 2.03 g) was added at once. The mixture was stirred for 72 h at 20 °C and was poured into 100 ml of ice water. After stirring for 2 h the white precipitate was filtered off and washed with 100 ml of water. The products were used without further purification. Yield 2.63 g (80%); mp >250 °C (decomp.); ^{1}H NMR ([D$_6$]-DMSO, 400 MHz) δ 4.02 (s, 6 H, CH_3), 8.39 (t, J = 7.81 Hz, 1 H, Ar–H{4}), 8.47 (d, J = 7.81 Hz, 2 H, Ar–H{3,5}), 12.08 (s, 2 H, NH); ^{13}C NMR ([D$_6$]-DMSO, 100.5 MHz) δ 34.64 (2 CH_3), 126.90 (2 Ar–CH{3,5}), 140.64 (Ar–CH{4}), 146.76 (2 Ar–C{2,6}), 149.80 (2 C=N), 162.88 (2 C=O); EI-MS *m*/*z* 329 (2%) $[H_2L^+]$.

H_2L/CD_3, 1/CD_3. The same ligand with both methyl groups fully deuterated was synthesised in the same way, using 1-trideuteromethyl-5-aminotetrazole (20 mmol, 2.04 g). Yield 1.88 g (57%); mp >250 °C (decomp.); ^{1}H NMR ($CDCl_3$–CF_3COOH, 400 MHz) δ 8.33 (t, J = 7.81 Hz, 1 H, Ar–H{4}), 8.60 (d, J = 7.81 Hz, 2 H, Ar–H{3,5}), due to the solvent the NH-protons cannot be determined; ^{13}C NMR ($CDCl_3$–CF_3COOH, 100.5 MHz) δ 35.50 (2 CD_3), 127.94 (2 Ar–CH{3,5}), 140.62 (Ar–CH{4}), 146.52 (2 Ar–C{2,6}), 149.36 (2 C=N), 162.09 (2 C=O); EI-MS *m*/*z* 336 (2%) $[H_2(L/CD_3)^+ + H]$.

$[Fe_3OL_3]$, 2.[12] To a solution of **1** (1.5 mmol, 494 mg) in 150 ml THF was added triethylamine (4.5 mmol, 455 mg, 0.63 ml) and $FeCl_3 \cdot 6H_2O$ (1.5 mmol, 405 mg). The mixture was heated for 5 days under reflux, cooled to 20 °C, and filtered. The solvent was removed under vacuum and the solid residue was dissolved in 200 ml trichloromethane. To remove $(HNEt_3)$-$[FeL_2]$, the organic phase was washed eight times with 200 ml portions of warm water (60 °C). The organic layer was separated, dried over sodium sulfate, and concentrated to 100 ml. While 200 ml of hexane were added, a crystalline product precipitated, which was filtered off and dried under vacuum (oil pump). The final product was **2**·6$CHCl_3$ — see syntheses of **3**–**5** below. Yield 245 mg (42%); mp >250 °C (decomp.); FAB-MS *m*/*z* 1166 (100%) $[Fe_3OL_3^+ + H]$.

$[Fe_3O(L/CD_3)_3]$, 2/CD_3. The deuteromethyl analogue of **2** was prepared in the same way using **1**/CD_3 (1.5 mmol, 503 mg). Yield 249 mg (41%); mp >250 °C (decomp.); FAB-MS *m*/*z* 1185 (100%) $[Fe_3O(L/CD_3)_3^+ + H]$.

$[Fe_2CoOL_3]$, 3; $[Fe_2NiOL_3]$, 4; $[Fe_2CuOL_3]$, 5. General procedure: To a solution of **1** (1.5 mmol, 494 mg) in 150 ml THF was added triethylamine (4.5 mmol, 455 mg, 0.63 ml), the appropriate metal chloride (1 mmol, 238 mg $CoCl_2 \cdot 6H_2O$, 238 mg $NiCl_2 \cdot 6H_2O$ or 171 mg $CuCl_2 \cdot 2H_2O$) and $FeCl_3 \cdot 6H_2O$ (1 mmol, 270 mg). The mixture was heated for 9 days under reflux, cooled to 20 °C, and filtered. The solvent was removed under vacuum, the solid residue was dissolved in 200 ml trichloromethane, and the organic phase was washed eight times with 200 ml portions of warm water (60 °C). The organic layer was separated, dried over sodium sulfate, and concentrated to 100 ml. On adding 200 ml of pentane or hexane, a crystalline product precipitated, which was filtered off and dried under vacuum (oil pump). **3**: Yield 146 mg (25%); mp > 250 °C

(decomp.); FAB-MS *m/z* 1169 (100%) [$Fe_2CoOL_3^+$ + H]. **4**: Yield 269 mg (46%); mp >250 °C (decomp.); FAB-MS *m/z* 1168 (100%) [$Fe_2NiOL_3^+$ + H]. **5**: Yield: 352 mg (60%); mp > 250 °C (decomp.); FAB-MS *m/z* 1173 (100%) [$Fe_2CuOL_3^+$ + H]. The solvent molecule content of the crystalline products was deduced from X-ray crystallography and found to depend on the choice of solvent used in the final precipitation step. For **2** and **5** this was hexane and the products were **2**·6$CHCl_3$ and **5**·6$CHCl_3$; for **4** it was pentane and the product was **4**·1.2$CHCl_3$·1.8C_5H_{12}. For **3** it was also hexane: the solvation was not determined but $CHCl_3$ was detected in the IR spectrum.

[$Fe^{III}_3OL_3$](NO_3), 6. To a solution of **2** (0.05 mmol, 58 mg) in 60 ml of dichloromethane was added dropwise a solution of $(NH_4)_2[Ce(NO_3)_6]$ (0.05 mmol, 28 mg) in 40 ml of methanol. The solution was stirred for 1 h at 20 °C and the solvent was removed under vacuum. The solid residue was extracted four times with 80 ml portions of dichloromethane. The organic phases were combined and concentrated to 40 ml. While 100 ml of hexane were added, a crystalline product precipitated, which was filtered off and dried under vacuum (oil pump). Yield 35 mg (57%); mp >250 °C (decomp.); FAB-MS *m/z* 1166 (100%) [$Fe_3OL_3^+$ + H].

($HNEt_3$)[$Fe^{III}L_2$], 7. To a solution of $FeCl_3$·$6H_2O$ (1 mmol, 270 mg) in 60 ml of dichloromethane was added a solution of **1** (2 mmol, 659 mg) in 100 ml of dichloromethane. After dropwise addition of triethylamine (4 mmol, 405 mg, 0.56 ml) the solution was stirred for 12 h at 20 °C. The solvent was removed under vacuum and the solid residue was dissolved in 20 ml trichloromethane. While 10 ml of diethyl ether were added, a crystalline product precipitated which was filtered off and dried under vacuum (oil pump). Yield: 710 mg (87%); mp >250 °C (decomp.); FAB-MS *m/z* 713 (100%) [FeL_2^- + $2H^+$]; 813 (30%) [$HNEt_3^+$ + FeL_2].

Spectroscopic methods

UV/VIS/NIR spectra were recorded on a Perkin-Elmer Lambda 9 spectrophotometer at room temperature in CH_2Cl_2 and $CDCl_3$ (Merck, Uvasol).

IR spectra of the complexes were recorded on a Mattson Galaxy series 4020 FTIR instrument, using KBr discs, at room temperature, and at 80 K for complexes **2**, **4** and **5**. Generally at low temperature, all peaks were shifted up by about 2 cm^{-1} and resolution of close peaks was improved, but the only additional peaks resolved were shoulders on one band in **2** and **4**, as noted below.

The inelastic incoherent neutron scattering (IINS) spectrum of complex **2** was run on TOSCA at the Rutherford Appleton Laboratory. The powdered sample, 0.23 g, was enclosed in aluminium foil, folded to fill the beam area, 5 × 2 cm, as evenly as possible. Data were treated using the standard in-house program GENIE.

Mössbauer spectra were recorded using a conventional spectrometer in the constant-acceleration mode. Isomer shifts are given relative to α-Fe at room temperature. The spectra obtained at 20 mT were measured in a He bath cryostat (Oxford MD 306) equipped with a pair of permanent magnets. The spectra were analysed by least-squares fits using Lorentzian line shapes.

NMR spectra were run on a Jeol JNM-GX-400 400 MHz spectrometer, at room temperature in $CDCl_3$. EI mass spectra were run on a Varian MAT 311A (70 eV), and FAB mass spectra on Micromass ZabSpec (Cs^+).

Electrochemistry and spectroelectrochemistry

Cyclic voltammetry at a platinum electrode was performed in CH_2Cl_2–TBAH (0.1 M, TBAH = [*n*-Bu_4N][PF_6]) at room temperature under nitrogen using a conventional undivided electrochemical cell with a three-electrode arrangement and a computer-controlled Amel 5000 system. Redox potentials were internally referenced against ferrocene/ferrocenium (Fc/Fc^+). CH_2Cl_2 for electrochemical experiments was refluxed and distilled over P_2O_5, stirred over K_2CO_3, deoxygenated with dry nitrogen and finally filtered over activated Al_2O_3 (Woelm Super I neutral) at −20 °C under an atmosphere of nitrogen. Tetra-*n*-butylammonium hexafluorophosphate was prepared and purified according to a previously described procedure.[16]

UV/VIS/NIR spectroelectrochemistry was performed at 290 K under nitrogen on solutions previously analysed by cyclic voltammetry. An electrochemical quartz cell with a three-electrode arrangement (gold minigrid as transparent working electrode), a Perkin-Elmer Lambda 9 spectrophotometer and an Amel 2053 potentiostat were used.[17]

For FTIR spectroelectrochemistry a BioRad FTS 155 spectrometer and Amel 2053 potentiostat were used. The novel spectroelectrochemical cell has been described recently.[18] For a spectroelectrochemical experiment, the analyte solution from cyclic voltammetry experiments (0.6 ml) was introduced with a syringe using Schlenk techniques. All spectra were recorded at room temperature under nitrogen at a resolution of 8 cm^{-1}. The argon-flushed empty sample compartment was used as background and the spectrum of analyte-free electrolyte solution was used to obtain corrected spectra.

Density functional calculations

DFT calculations were performed on a model of the mixed-valence iron complex **2**, at the B3LYP level[19] using the Gaussian-98 package.[20] Although the molecule is extremely large for calculations at this level it was decided not to simplify it drastically because the electronic structure of the ligand system was expected to influence the properties of the Fe_3O core significantly. Therefore, coordinates were taken from the X-ray analysis,[12] but with hydrogens substituted for the methyl groups and one of the iron atoms slightly displaced (by 0.01 Å along the O–Fe vector) in order to lower the molecular symmetry from D_3 to C_2 and allow the density matrix to reproduce the properties of a not fully valence-delocalised molecule. Since the calculations are very time-consuming we did not attempt to optimise the geometries, and we used the rather small LANL2DZ basis set with a non-relativistic effective core potential (ECP) at the iron atoms.[21] Spin states $S = 0$, $S = 1$ and $S = 2$ were calculated and converged to 10^{-6}.

Crystal structure analysis

Crystal data for 4·1.2$CHCl_3$·1.8C_5H_{12}. $C_{43.2}H_{49.8}Cl_{3.6}Fe_2N_{33}NiO_7$, M = 1441.39. Crystal dimensions: 0.8 × 0.6 × 0.5 mm, trigonal, space group $R3c$ (no. 161 of ref. 22): a = 2.3184(3), c = 22.634(3) Å, V = 10536(2) $Å^3$, Z = 6. Diffractometer: Stoe-Siemens-Huber, fitted with a graphite monitor and Siemens SMART CCD area detector. Radiation: Mo-Kα, λ = 0.71073 Å, T = 133(2) K. Measurement details: φ and ω scan, range 35° ≤ 2θ ≤ 56.5°, section of the reciprocal lattice h = −26 to 0, k = 0 to 30, l = 0 to 30. A total of 42727 reflections were measured, of which 2902 were considered independent, and 2452 were considered observed as defined by $I > 2(\sigma)I$. Linear absorption coefficient: 0.877 mm^{-1}, absorption correction: semi-empirical from equivalents. The largest residual density was 0.388 e $Å^{-1}$. Refined parameters: 245, $R1$ = 0.0371, $wR2$ = 0.1047 (all data). The structure was solved by direct methods (ref. 23) and refined with all data by full-matrix-least-squares on F^2 using SHELXL-97 (ref. 24*c*). Non-hydrogen atoms were refined anisotropically. For the hydrogen atoms the riding model was used. The solvent molecules are severely disordered. They were refined with distance restraints and restraints for the anisotropic displacement parameters to give the formula indicated here.

Table 1 Metal–metal distances (Å) in $M^{III}_2M^{II}O$ clusters

	Mean	Ref.
$[Fe_3OL_3]$, **2**	3.267	12
$[Fe_2NiOL_3]$, **4**	3.282	[a]
$[Fe_2CuOL_3]$, **5**	3.287	[a]
$[Fe^{III}_2Fe^{II}O(O_2CMe)_6(py)_3](py)$	3.308	26
$[Fe^{III}_2Co^{II}O(O_2CMe)_6(py)_3](py)$	3.306	26

[a] This work—see crystallographic data.

Crystal data for 5·6CHCl$_3$. $C_{39}H_{33}Cl_{18}CuFe_2N_{33}O_7$, M = 1889.32. Crystal dimensions: 0.3 × 0.3 × 0.35 mm, trigonal, space group $R3c$ (no. 161 of ref. 22): a = 23.314(3), c = 22.811(3) Å, V = 10808(2) Å^3, Z = 6. Diffractometer: Nonius Kappa CCD area detector. Radiation: Mo-Kα, λ = 0.71073 Å, T = 173(2) K. Measurement details: ω scan, range 1.75° ≤ θ ≤ 22.51°, section of the reciprocal lattice h = −30 to 30, k = −30 to 26, l = −29 to 28. A total of 6804 reflections were measured, of which 2337 were considered independent, and 1356 were considered significant as defined by $I > 2(\sigma)I$. Linear absorption coefficient: 1.436 mm^{-1}, absorption correction: Scalepeak. Refined parameters: 132, $R1$ = 0.0629, $wR2$ = 0.1347 (all data). The structure was solved by direct methods (ref. 23) and refined with all data by full-matrix-least-squares on F^2 using SHELXL-97 (ref. 24c). Non-hydrogen atoms were refined anisotropically. For the hydrogen atoms the riding model was used. The solvent molecules are severely disordered. They were refined with distance restraints and restraints for the anisotropic displacement parameters to give the formula indicated here.

CCDC reference numbers 165605 and 153559.

See http://www.rsc.org/suppdata/dt/bl/b100780g/ for crystallographic data in CIF or other electronic format.

Results

Structures

The molecular structure shown in Fig. 1 was established by crystallography for the mixed-valence iron complex **2**[12] and mixed-metal iron–nickel and iron–copper complexes **4**, **5**;[25] and using the solid state IR spectra for the iron–cobalt complex **3** and the oxidised, tri-iron(III) complex **6**. In solution, the electrochemical data indicate facile electron transfer involving the couples $Fe^{III}_3/Fe^{III}_2Fe^{II}$ and $Fe^{III}_2Co^{III}/Fe^{III}_2Co^{II}$, and also $Fe^{III}_2M^{II}/Fe^{III}Fe^{II}M^{II}$, (M = Fe, Co, Ni, Cu), and hence imply similar structures for the oxidised and reduced forms of these complexes, with little if any ligand rearrangement accompanying the electron transfers.

The four neutral complexes crystallise with solvent molecules depending on the conditions of preparation as noted above. The molecular point group is D_3; thus in each complex the three metal ions are indistinguishable, and the central metal oxygen units are planar by imposed symmetry. The complex molecules, which are stacked on threefold axes in the crystal, are strongly chiral, the central pyridine unit of each ligand being inclined to the metal triangle plane (at 33.3° in **4**), so that the tetrazolyl donor units of each ligand are directed from opposite sides of the plane. The overall size of the metal atom triangle as measured by the mean metal–metal distance in the Fe_2M units does not vary significantly with different metals M, but it is apparently affected by the ligand, being slightly less than in the carboxylate-bridged complexes with the same central metal–oxygen clusters (Table 1).

Vibrational spectra—solid state

IR spectra of the mixed-valence complex **2** are compared with spectra of other complexes in the range 1000–400 cm^{-1} in Fig. 2 and 3. Selected frequencies and assignments are listed in Table 2.

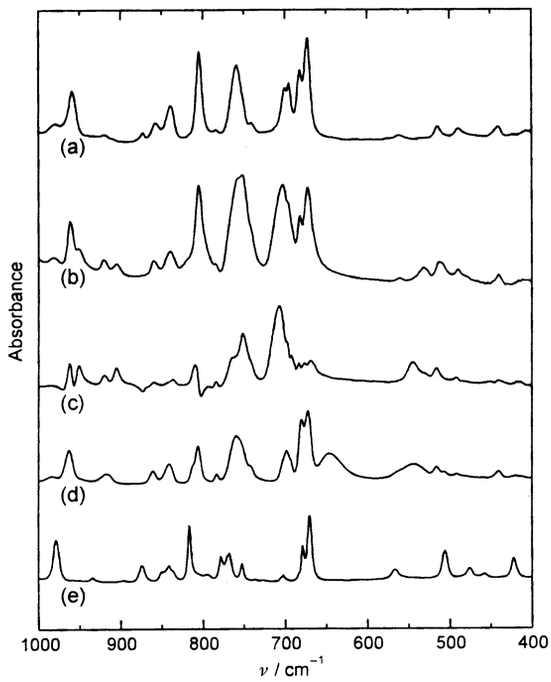

Fig. 2 IR spectra of **2**–**5** and $(HNEt_3)(Fe^{III}L_2)$, 1000–400 cm^{-1}. T = 298 K, KBr disc. (a) $[Fe_3OL_3]\cdot 6CHCl_3$; (b) $[Fe_2CoOL_3]\cdot xCHCl_3$; (c) $[Fe_2NiOL_3]\cdot 1.2CHCl_3\cdot 1.8C_5H_{12}$ "corrected" by subtraction of a spectrum of $[Fe_3OL_3]\cdot 6CHCl_3$; (d) $[Fe_2CuOL_3]\cdot 6CHCl_3$; (e) $(HNEt_3)[Fe^{III}L_2]$.

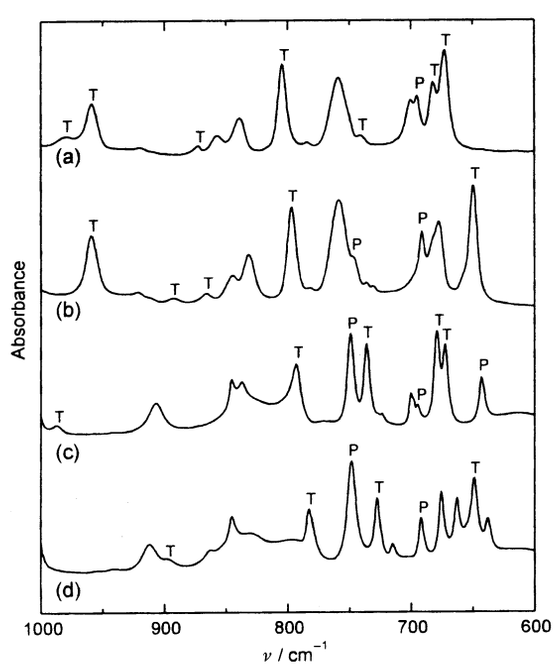

Fig. 3 IR spectra, 1000–600 cm^{-1}. T = 298 K, KBr disc. (a) $[Fe_3OL_3]\cdot 6CHCl_3$; (b) $[Fe_3O(L/CD_3)_3]\cdot 6CHCl_3$; (c) H_2L; (d) $H_2(L/CD_3)$. T: features assigned to the tetrazole units (including substituents). P: features assigned to the pyridine rings and H atoms of the dipicolinate residue.

Here we concentrate on the identification of metal–oxygen stretch frequencies. Criteria for assignment include deuteration shifts, IINS intensities, and comparisons with well-analysed spectra of related molecules.[27–31]

In the chloroform solvate of **2**, the strong band at 759 cm^{-1} contains intensity due to $\nu_{as}(CCl_3)$ but quantitative comparisons with the $CDCl_3$ analogue showed that the predominant absorption is due to features other than chloroform. Also at low temperature the two bands in the $CHCl_3$ solvate were partly

Table 2 Summary of vibrational frequencies (600–850 and 1350–1660 cm^{-1}) and assignments for complexes $[Fe_2MOL_3]$

$[Fe_3OL_3]$ **2** IINS	$[Fe_3OL_3]$ **2** IR	$[Fe_2CoOL_3]$ **3** IR	$[Fe_2NiOL_3]$ **4** IR	$[Fe_2CuOL_3]$ **5** IR	Assignments[a]
sh				646br	ν_{as}(MO)
sh	673	672	673	672	tetrazole ring
sh	682	681	682	680	tetrazole ring
692s	695		697sh	698sh	py ring ν_{26}
		703	703		ν_{as}(MO)
	742		740sh[e]	740sh	tetrazole ring
750s		747sh	752		py ring γ(CH)
	≈755[b]	752	≈760		ν_{as}(MO)
	759[c,d]	≈760	759	759	$\nu_{as}(CCl_3)$
780m	784	785	783	783	
811w	805	805	805	805	tetrazole ring[f]
	839	837	838	840	
850br m	857	859	861	863	py ring γ(CH)
	872				CH_3 rock?[f,g]
1363w	≈1350	1348	≈1350	≈1358	amide II
1450vs	1445	1446	≈1445	1454??	CH_3 asymmetric bend[g]
1484					
	1602	1602	≈1602	≈1603	py ring ν_{8a}
1630br					
	1662	1662	≈1655	1660	amide I

[a] py = pyridine ring of ligand H_2L; bands numbered ν_{8a}, ν_{26} are correlated with those of pyridine itself, in the scheme of ref. 28; amide = –CO–N^-– unit; bands numbered I, II, in the scheme of ref. 29. [b] Overlaid by $\nu_{as}(CCl_3)$ but also strong when $\nu_{as}(CCl_3)$ is shifted by deuteration—see discussion. Presumably also coincides with γ(CH). [c] Shifts to *ca.* 735 cm^{-1} in the $CDCl_3$ solvate. [d] Shoulder *ca.* 770 cm^{-1} at T = 80 K. [e] More pronounced at 742 cm^{-1}, at T = 80 K. [f] Present in 1-methyl-5-aminotetrazole, not in dipicolinic acid. Assignment consistent with ref. 23. [g] Assigned on basis of CH_3/CD_3 shifts.

resolved. As noted above, the Fe_2Ni complex **4** was contaminated with **2**. With appropriate subtraction it was possible to eliminate features of **2** without introducing any obvious over-subtractions, at least in the range 850–400 cm^{-1}. The corrected spectrum is shown in Fig. 2. The main effect of subtraction is to resolve more clearly the pyridine mode at 752 cm^{-1}, and the broad shoulder at 760 cm^{-1}. The Fe_2Co and Fe_2Cu complexes were more pure, and the spectra shown in Fig. 2 are uncorrected. The sample of the oxidised complex $[Fe^{III}{}_3OL_3](NO_3)$, **6**, was found to be more significantly mixed with **2**, and it was not possible to separate the pure spectrum on the basis of any unique peaks.

In the range 500 to 700 cm^{-1}, and likewise in the IINS spectrum of **2**, the strongest peaks were mostly assignable to well-defined ligand vibrations. All complexes show a strong peak at *ca.* 760 cm^{-1} which we assign as $\nu_{as}(Fe_2MO)$. The expected second component of this vibration has been assigned in the mixed-metal complexes at 703 cm^{-1} (Fe_2CoO, Fe_2NiO) and 646 cm^{-1} (Fe_2CuO). In the mixed-valence complex **2** it is not seen and the only likely region where it could be obscured is 650 to 700 cm^{-1}.

IR of 2 in solution: spectroelectrochemistry

IR spectra for progressive oxidation and reduction of **2** in solution are shown in Fig. 4. Both electrochemical processes could be driven in either direction and yielded consistent spectra, the cation $[Fe_3O]^+$ in particular being stable in solution, even though the spectra confirmed that the solid preparations of **6** contained a significant fraction of **2**. Metal–oxygen stretches could not be monitored in solution owing to strong solvent absorptions but the effect of redox state on the amide-I band is clear. This band is broad in **2**, but on oxidation it sharpens and shifts to higher energy by almost 30 cm^{-1}, whereas on reduction it broadens and shifts to lower energy by about 20 cm^{-1}. Further reduction produced changes which were qualitatively similar, finally yielding two broad and poorly resolved bands for the homovalent dianion $[Fe^{II}{}_3OL_3]^{2-}$. Spectra of the four oxidation states from $[Fe^{III}{}_3OL_3]^+$ to $[Fe^{II}{}_3OL_3]^{2-}$ are compared in Fig. 5.

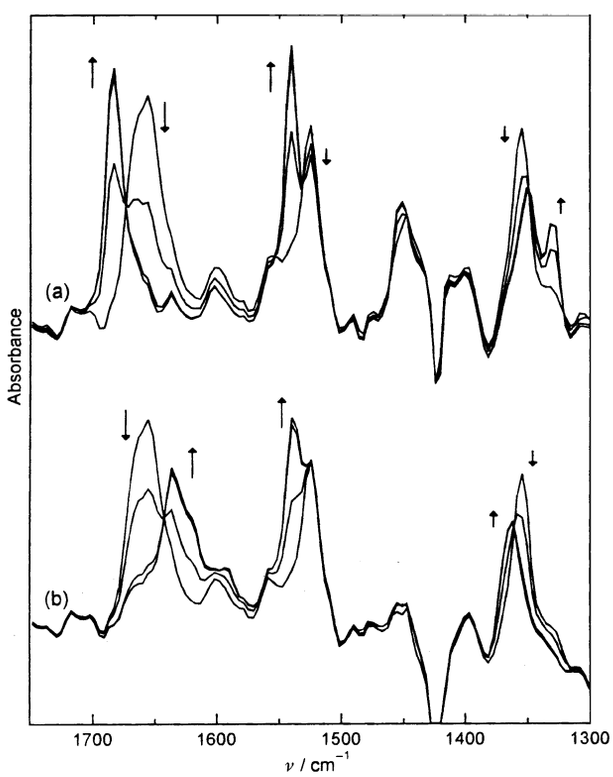

Fig. 4 IR spectral changes during oxidation and reduction of $[Fe_3OL_3]$ in CH_2Cl_2, T = 298 K. Successive spectra were collected at constant time intervals (15 s) and constant electrochemical potential: (a) E = 250 mV *vs.* Fc/Fc^+, (b) E = −850 mV *vs.* Fc/Fc^+. The arrows indicate the direction of the spectral changes.

Electrochemistry

All electrochemical data that can be ascribed to well-defined electrode processes are summarised in Table 3. The expected impurity signals in the voltammograms of **4** and **5** were easily distinguished. The tri-iron complex **2** shows three distinct one-electron processes (Fig. 6): a reversible oxidation at +85 mV, a

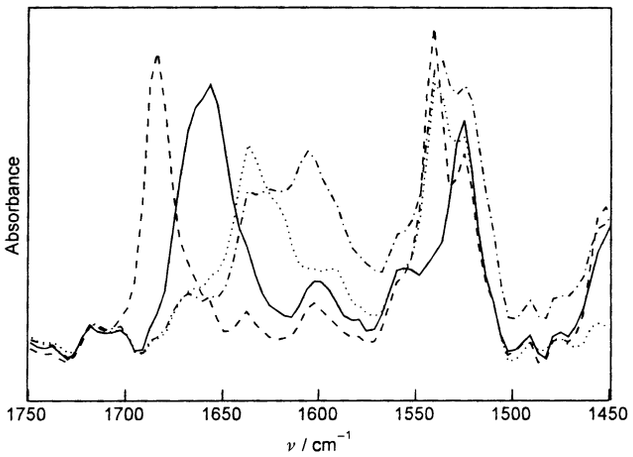

Fig. 5 IR spectra of the four redox states of $[Fe_3OL_3]$ recorded during electrochemical oxidation/reduction in CH_2Cl_2, T = 298 K. $[Fe_3OL_3]^+$ (dashed line), $[Fe_3OL_3]$ (solid line), $[Fe_3OL_3]^-$ (dotted line), $[Fe_3OL_3]^{2-}$ (dotted-dashed line).

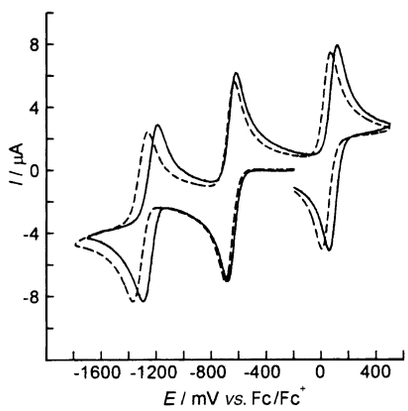

Fig. 6 Cyclic voltammograms of $[Fe_3OL_3]$, **2**, (solid line) and $[Fe_2CoOL_3]$, **3**, (dashed line) in CH_2Cl_2. T = 298 K, scan rate 50 mV s^{-1}.

Table 3 Half-wave potentials (E/mV, *vs.* Fc/Fc^+) for complexes $[Fe_2MOL_3]$[a]

M	Fe	Co	Ni	Cu	Notes
$[Fe_2MOL_3]^{+/0}$	85	35	[b]	[b]	[c]
$[Fe_2MOL_3]^{0/-1}$	−635	−660	−725	−550	[c]
$[Fe_2MOL_3]^{0/-2}$	−1230	−1310	−1425	−1220	[d]

[a] Cyclic voltammetry in CH_2Cl_2—0.1 M TBAH; scan rate 50 mV s^{-1}. [b] Also very weak signal at 70 mV assigned to impurity $[Fe_3OL_3]$. [c] Reversible, ΔE_p = 60 ± 10 mV. [d] Quasi-reversible, ΔE_p = 100 ± 10 mV.

reversible reduction at −635 mV and a quasi-reversible reduction at −1230 mV with peak potential separation of 100 mV at a scan rate of 50 mV s^{-1}. The Fe_2Co complex **3** has three similar processes: reversible oxidation at +35 mV, reversible and quasi-reversible reduction at −660 and −1310 mV (Fig. 6). Assignment of the first of these three as an electron transfer at the cobalt centre is supported by comparisons of $Co^{III/II}$ and $Fe^{III/II}$ potentials for a series of mononuclear complexes. The difference varies strongly with ligand environment, in a sequence from weak-field to strong-field ligands.[32] As applied to complexes **2** and **3** this difference measures the equilibrium:

$$Fe^{III}{}_2Co^{III} + Fe_3 \rightleftharpoons Fe^{III}{}_2Co^{II} + Fe^{III}{}_3 \qquad (1)$$

where only the unambiguous oxidation states are shown. The Fe_2Ni and Fe_2Cu complexes **4** and **5** are reduced at −725 and −550 mV, respectively, with a second quasi-reversible reduction

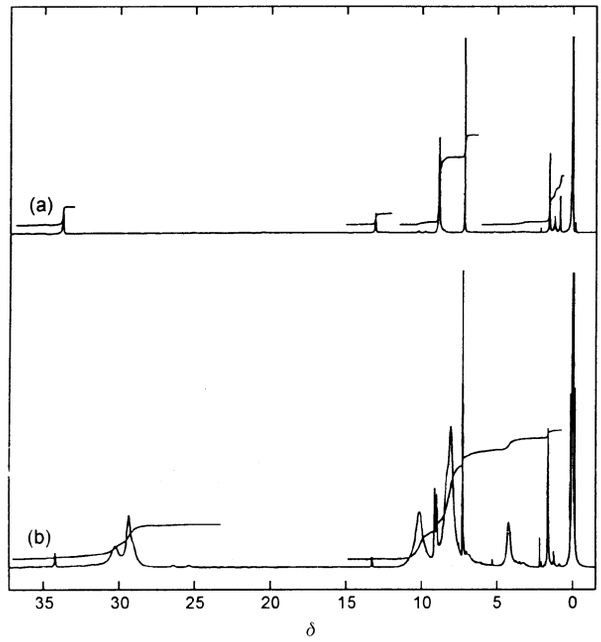

Fig. 7 ^1H NMR spectra (270 MHz, in $CDCl_3$, T = 298 K). (a) $[Fe_3OL_3]$, **2**; (b) $[Fe_2CuOL_3]$, **5**.

at −1425 and −1220 mV, respectively. These complexes are not electroactive at moderate anodic potentials.

NMR spectra

Proton NMR spectra of the mixed-valence complex **2** and the Fe_2Cu complex **5** are compared in Fig. 7. Chemical shifts and assignments are listed in Table 4. Apart from solvent peaks, the spectrum of **2** shows the three sharp and well separated peaks expected for protons of one set of equivalent CH_3 groups and one set of equivalent pyridine rings (H in *meta* and *para* positions). Shifts and linewidths are similar to those reported for complexes $[Fe_3O(OOCR)_6(py)_3]^{n+}$ (n = 0, 1) in solution at room temperature.[10,39] The spectrum of **5** shows traces of **2** as impurity, but otherwise, the proton peaks of **5** appear in slightly different positions from **2**, and each is composite. The band profile for the *meta* protons of the pyridine residue clearly shows an overlap of three peaks of similar intensity, two of similar width and one narrower, though all three are considerably broader than in **2**. The profile for the methyl groups is equally clear, again with one sharper and two broader bands. These are the profiles expected for C_2 symmetry in the heterometallic complex.

Electronic spectra

Complex **2** shows absorption bands over all the measured wavelength region up to 2300 nm (Fig. 8). Additional weak and broad, and thus unresolved, bands are present, some of them at longer wavelengths, but the main feature, unique to the mixed-valence complex **2**, is the band at 1680 nm (6000 cm^{-1}), clearly demonstrated by the differences between successive spectra during electrochemical oxidation, as well as by comparison with the mixed-metal complexes **3**–**5** (Table 4). None of the bands of **2** seems to be significantly solvatochromic when going from CH_2Cl_2 to CH_3CN. As regards the oxidised complex **6**, again the contamination of the prepared sample with **2** prevented direct observation of the spectrum, but again it was successfully measured by spectroelectrochemistry. Progressive oxidation of **2** gave progressive changes in the spectrum, and the reverse changes were seen on re-reduction. During the oxidation the near-IR bands disappear completely, finally yielding a spectrum with maxima at 258 and 480 nm (Fig. 8). Reversible reduction to the iron(III,II,II) mixed-valence anion

Table 4 Proton NMR chemical shifts (ppm) in oxo-centred trinuclear complexes [a]

	Pyridine-H *ortho*	*meta*	*para*	Alkyl-H CH_3
$[Fe_3OL_3]$	—	34.2	13.3	9.0
$[Fe_2CuOL_3]$	—	30.3	4	10.3
	—	29.3		8.3
	—	29.0		8.0
$[Fe_3O(OOCCMe_3)_6(py)_3]^+$ [b]	63.9	27.8	Obscured	8.1
$[Fe_3O(OOCCMe_3)_6(py)_3]$ [b]	—	17	8.8	4.4

[a] In $CDCl_3$, T = 298 K. [b] Ref. 10.

Table 5 Absorption maxima (λ/nm) of complexes $[Fe_2MOL_3]^{n+}$ [a]

$[Fe_3OL_3]$ **2**	$[Fe_3OL_3]^+$ $\mathbf{2}^+$ [b]	$[Fe_3OL_3]^-$ $\mathbf{2}^-$ [b]	$[Fe_2CoOL_3]$ **3**	$[Fe_2NiOL_3]$ **4**	$[Fe_2CuOL_3]$ **5**
268, 425, 742, 900sh, 1680, 1900sh	258, 460sh, 480	269, 375sh, 585, 730sh, ≈1300 [c]	267, 428, 500sh, 580sh, 735sh	257sh, 266, 424, 560sh, 820, 1680 [d]	260, 290sh, 330sh, 438, 675sh, 1680 [d]

[a] In CH_2Cl_2, T = 298 K. [b] In CH_2Cl_2–0.1 M TBAH, T = 290 K. [c] Weak and not well characterised. [d] Very weak signal assigned to impurity **2**.

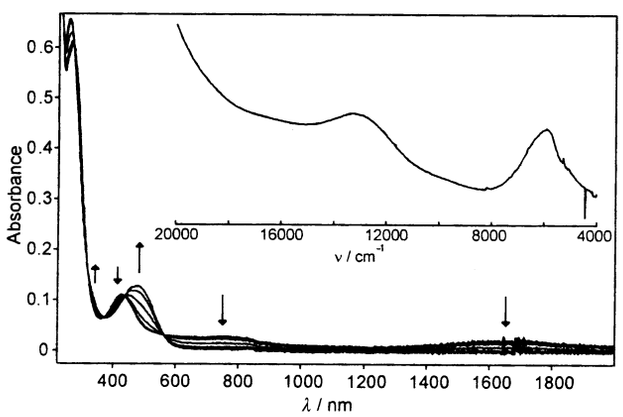

Fig. 8 Electronic spectra of $[Fe_3OL_3]$ and $[Fe_3OL_3]^+$, in CH_2Cl_2. T = 290 K. The arrows indicate the direction of spectral changes during the electrochemical oxidation of $[Fe_3OL_3]$. Spectra were collected at the following potentials: −60, −20, 20, 60, 100, 140 mV *vs.* Fc/Fc^+. Inset: A more detailed view of the NIR bands of $[Fe_3OL_3]$, in $CDCl_3$, T = 298 K.

$[Fe_3OL_3]^-$ is also accompanied by almost complete disappearance of NIR bands, as well as a strong shift of UV/VIS bands. The final spectrum consists of narrow bands at 269 and 585 nm along with broad signals in the same region and probably a very weak absorption at 1300 nm. Further reduction, to $[Fe_3OL_3]^{2-}$, led to a further decrease of absorption in the NIR region, but the limited stability of the fully reduced species did not allow complete spectral characterisation. Table 5 shows the spectra of all the observed redox states of complex **2**.

Mössbauer spectra

Observed and fitted Mössbauer spectra of **2** are shown in Fig. 9 and 10; Fig. 9 giving representative spectra of the solid at three temperatures, Fig. 10 giving spectra of frozen solutions in THF. Isomer shifts and quadrupole splittings of all complexes are listed in Table 6. The complexes expected to contain only trivalent iron, *i.e.* mixed-metal **3**, **4** and **5** and fully oxidised **6**, all have similar values of δ, in the range 0.44 to 0.47 mm s^{-1}. Analyses of numbers and widths of peaks in all the other spectra were based on extensive trials of alternative schemes, subject only to the usual constraint that all spectra are expected to consist of overlays of doublets due to quadrupole splitting. The relatively broad line widths of $[Fe^{III}_2Co^{II}OL_3]$, $[Fe^{III}_2Cu^{II}OL_3]$ and $[Fe^{III}_3OL_3]$ are probably due to the onset of magnetic broadening at low temperature. In the spectra of the

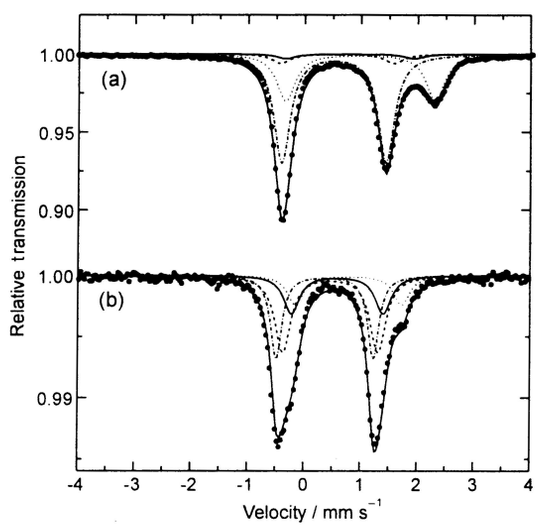

Fig. 9 Mössbauer spectra of $[Fe_3OL_3]$, **2**, in the solid state. (a) T = 4.2 K, (b) T = 332 K. Field 20 mT perpendicular to the γ-beam. Broken lines are Lorentzians fitted for four quadrupole doublets.

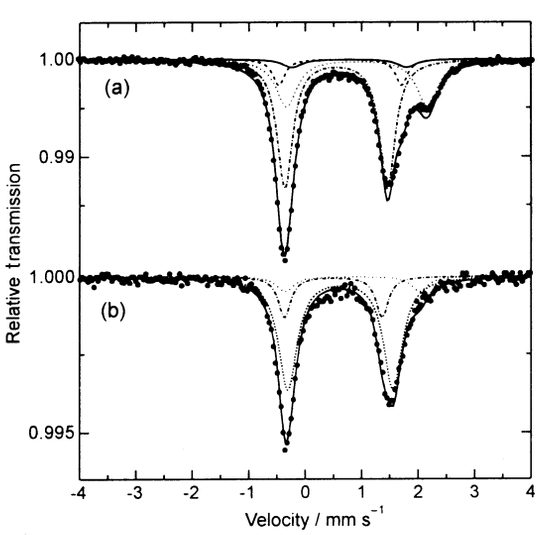

Fig. 10 Mössbauer spectra of $[Fe_3OL_3]$, **2**, in frozen THF. (a) T = 4.2 K and (b) T = 160 K with a field of 20 mT perpendicular to the γ-beam. Broken lines are Lorentzians fitted for three quadrupole doublets.

Table 6 Mössbauer parameters of complexes $[Fe_2MOL_3]$, **2**–**5**, and $[Fe_3OL_3](NO_3)$, **6**

	T/K	δ/mm s^{-1} [a]	ΔE_Q/mm s^{-1} [a]	Γ/mm s^{-1} [b]	Relative contribution (%)
Iron(III) complexes					
$[Fe_2CoOL_3]$, **3**	4.2	0.46	1.79	0.60	100
$[Fe_2NiOL_3]$, **4**	4.2	0.46	1.75	0.38	100
$[Fe_2CuOL_3]$, **5**	4.2	0.47	1.53	0.90	100
$[Fe^{III}{}_3OL_3](NO_3)$, **6**	4.2	0.44	1.10	0.66	100
$[Fe_3OL_3]$, **2**, solid state					
I	4.2	0.52	1.85	0.34	60
II		0.99	2.65	0.40	30
III		0.58	2.00	0.40	7
IV		0.80	2.27	0.40	3
I	332	0.37	1.72	0.24	30
II		0.79	1.88	0.34	15
III		0.47	1.69	0.34	37
IV		0.59	1.62	0.34	18
$[Fe_3OL_3]$, **2**, THF solution					
I	4.2	0.55	1.83	0.36	60
II		0.91	2.50	0.47	30
M		0.66	2.11	0.28	10
I	160	0.50	1.73	0.27	18
II		0.84	2.39	0.36	9
M		0.62	1.87	0.40	73

[a] Standard deviation 0.01 mm s^{-1}. [b] Standard deviation 0.01–0.04 mm s^{-1}, depending on value of Γ.

mixed-valence complex **2**, generally four doublets were required as discussed below. In the frozen solution of **2** in THF, only three doublets were required, one of which, increasing in strength with increasing temperature, has $\delta = 0.66$ mm s^{-1} at 4.2 K and $\delta = 0.62$ mm s^{-1} at 160 K. The change in δ with temperature is attributed to the second-order Doppler effect; estimates of δ_{SOD} are in the range 0.05 to 0.1 mm s^{-1},[40] and a value of 0.04 mm s^{-1}, gives our experimental value $\delta = 0.62$ mm s^{-1} at 160 K.

Discussion

As noted above, the crystal structures of at least two of the mixed-metal complexes show threefold symmetry, one of them being the $Fe^{III}{}_2Cu^{II}$ complex, in which presumably the copper(II) centres are subject to Jahn–Teller distortion. This emphasises the ability of the ligand to conceal asymmetry by rotational disorder. It is not surprising therefore that the mixed-valence compound **2** also shows apparent threefold symmetry, regardless of whether this is due to disorder or valence delocalisation.

It is not possible to estimate distances in $[Fe^{III}{}_2Fe^{II}OL_3]$, *i.e.* the hypothetical valence-localised form of complex **2**, but it is possible to make the corresponding estimate in two complexes of the carboxylate series. The mixed-valence complex $[Fe^{III}{}_2Fe^{II}(OOCMe)_6(3\text{-Etpy})_3]\cdot 0.5C_6H_5CH_3$ apparently shows complete valence localisation,[41] and in $[Cr^{III}{}_2Co^{II}O(OOCCMe_3)_6(py)_3]\cdot(py)$, the Cr–O and Co–O distances were distinguished by EXAFS, though rotationally disordered in the crystal.[42] The distortions of the metal-ion triangle from equilateral to isosceles are similar, though differently expressed. In the $Cr^{III}{}_2Co^{II}$ complex, by describing the triangle as approximately equilateral, the displacement of the oxygen atom from the centre could be estimated as 0.05 Å; in the $Fe^{III}{}_2Fe^{II}$ complex the metal–metal distances could be measured independently and the corresponding displacement is about 0.10 Å.

Temperature-dependent magnetisation measurements support the assignment of the component oxidation states in **2** with antiferromagnetic coupling.[13] Using the HDVV spin-only model with the Hamiltonian:

$$H^{i}_{ex} = -2\,J_{ab}\,\boldsymbol{S}_a\cdot\boldsymbol{S}_b - 2\,J\,(\boldsymbol{S}_a\cdot\boldsymbol{S}_c + \boldsymbol{S}_b\cdot\boldsymbol{S}_c) \qquad (2)$$

where $S_a = S_b = 5/2$ and $S_c = 2$ are the spins at the Fe^{3+} and Fe^{2+} sites, at temperatures 4.2 to 295 K gave a good fit with $J_{ab} = -70$ cm^{-1}, $J = -24.5$ cm^{-1}. For the complex $[Fe_3O(OOCCMe_3)(py)_3](py)$ neutron scattering spectra have been fitted with $J_{ab} = -60$ cm^{-1}, $J = -18$ cm^{-1}, though some evidence of mixing of energy levels was also presented.[43] The more negative values for the present complex **2** are consistent with the shorter interatomic distances; and the difference ($J_{ab} - J$), being similar in both cases, implies that the deviations from threefold symmetry, though concealed, are similar in both clusters.

The IR spectra show conclusively that the central metal ion triangle in the mixed-valence complex $[Fe_3OL_3]$, **2** does not have threefold symmetry on the vibrational time scale, either in the solid state (from 80 K upwards) or in solution at room temperature. This is most clearly demonstrated by the spectroelectrochemistry of **2** in solution, showing the contrast of the sharp amide-I band in the oxidised complex $[Fe_3OL_3]^+$ with that of the mixed-valence complex. These observations indicate inequivalence of the iron sites, *i.e.* at least some degree of valence localisation, but they do not indicate the degree of localisation, nor do they exclude dynamic delocalisation, except to say that this must be slower than the time scale of vibrational spectroscopy. From the solution NMR spectra however it is equally clear that dynamic delocalisation, *i.e.* intramolecular electron transfer, does take place, in solution, at a rate faster than the NMR time scale, at room temperature.

Returning to the IR spectra, it may be significant that only one component of the asymmetric metal cluster vibration $\nu_{as}(Fe_3O)$ is seen in the solid state spectra, but the complexity of the spectra in the relevant region leaves open the possibility that the lower-frequency component is present. What can be said, from the data summarised in Table 7, is that any splitting between the two components of $\nu_{as}(Fe_3O)$ must be considerably less than in the carboxylate-bridged complexes. The same is true for the mixed-metal Fe_2M complexes and it may be a consequence of the different ligand environments rather than the electronic character of the mixed-valence cluster.

From the electrochemical properties of the complexes two comproportionation constants can be obtained as follows:

Table 7 Frequencies (cm^{-1}) of components of $\nu_{as}(Fe_2MO)$ in oxo-centred trinuclear complexes

		ν_{as}/cm^{-1}	Ratio	Ref.
$[Fe_3OL_3]\cdot 6CHCl_3$, **2**	760	700/670	1.09/1.13	This work
$[Fe_3O(OOCMe)_6(py)_3](py)$	695	570	1.22	44
$[Fe_3O(OOCCMe_3)_6(py)_3]$	705	580	1.22	9, 39
$[Fe_2NiOL_3]\cdot 6CHCl_3$, **4**	760	705	1.08	This work
$[Fe_2NiO(OOCMe)_6(py)_3](py)$	722	565	1.28	44
$[Fe_2NiO(OOCCMe_3)_6(py)_3]$	721	595	1.21	45

$$[Fe^{III}{}_3OL_3]^+ + [Fe_3OL_3]^- \rightleftharpoons 2\,[Fe_3OL_3],\ K_{com}{}^{Fe} \quad (3)$$

$$[Fe^{III}{}_2Co^{III}OL_3]^+ + [Fe_2Co^{II}OL_3]^- \rightleftharpoons 2\,[Fe^{III}{}_2Co^{II}OL_3],\ K_{com}{}^{Co} \quad (4)$$

with $K_{com}{}^{Fe} = 2 \times 10^{12}$, $K_{com}{}^{Co} = 7 \times 10^{11}$. Here only the unambiguous oxidation states of iron are indicated. Both constants are large but in view of the different ionic charges they are likely to be dominated by environmental effects, especially solvation.[46] Iron(III,II) mixed-valence species are involved in both reactions. If iron(III/II) delocalisation is important, it will tend to increase $K_{com}{}^{Fe}$ and decrease $K_{com}{}^{Co}$, relative to the values expected for full localisation.

Intervalence charge-transfer is a well-known test of valence delocalisation. In the present series of complexes a band at 6000 cm^{-1} is unique to the mixed-valence complex **2**. We interpret this cautiously since it is partly overlapped, and also because of the other weaker absorptions observed at lower energies. Nevertheless it is clear that the 6000 cm^{-1} band is much narrower than calculated for a localised intervalence transition (the Hush formula[47] gives the full width at half height, 3700 cm^{-1}, compared with *ca.* 2000 cm^{-1}, observed) and no solvatochromism was detected. This indicates significant static valence delocalisation, though not necessarily the full extent of delocalisation defined as Robin–Day class III:[48] recent arguments by Lambert and Nöll indicate that a class III/II borderline state is consistent with the spectrum.[3g] (The fact that the further reduced complex $[Fe_3OL_3]^-$, assigned as iron(III,II,II), shows no low-energy IT band probably indicates some structural modification).

The most direct indications of the mixed-valence character of the tri-iron cluster are the Mössbauer spectra, and here the results are in complete contrast with earlier work on the carboxylate-bridged series.[13] Over the temperature range 4.2 to 332 K, all solid state spectra of **2** were adequately fitted with two pairs of Lorentzian lines, consistent with two sets of mixed-valence molecules coexisting. A linear interpolation of isomer shifts between those determined for pure iron(III) and iron(II) in comparable ligand environments[49] gave fractional oxidation states for the two components, *i.e.* Fe(2.9+, 2.9+, 2.2+) and Fe(2.75+, 2.75+, 2.5+) the proportion of the latter increasing with increasing temperature. Band shapes gave no sign of temperature-dependent lifetime broadening. For each of the two components, this is consistent with either of the two limiting situations described above, *i.e.* static or dynamic, where dynamic in this case means faster than the Mössbauer time scale. The static option was preferred for both components, leading to the paradox of a system which shows some valence delocalisation at 4.2 K, yet does not achieve complete delocalisation at room temperature. It was argued that by a suitable blend of three known mechanisms of electronic interaction, the paradox could be resolved. Starting as above from the assignment of high-spin Fe(3+, 3+, 2+) for the basis electronic state, the spin-only model (eqn. (2)) gives a ground state (S, S_{ab}) = (1,1) for the trinuclear cluster, and states (2,0), (2,1), (0,2) located at energies 7, 100 and 130 cm^{-1} above the ground state (Fig. 11). Double exchange leads to a splitting of each of the spin-only states into A and E components, and it was shown that for the second and third excited states, the splitting is both

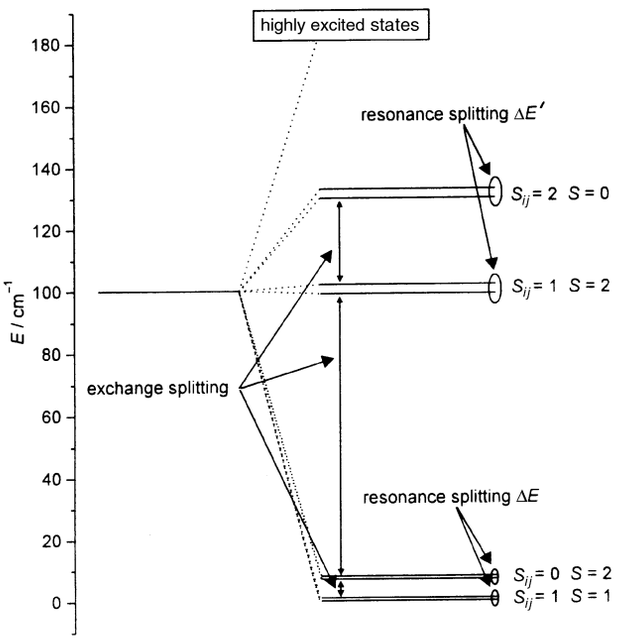

Fig. 11 Resonance-exchange levels of $[Fe_3OL_3]$, **2**, for the case of weak double-exchange interaction.

stronger and less sensitive to symmetry distortions, than it is for the ground and first excited states. It is this difference that justifies the use of the fully localised valence model to treat the magnetisation data, while double-exchange is still strong enough to cause significant partial valence delocalisation, affecting the spectra.

The almost complete localisation of the extra electron in the ground state is of course explained by vibronic interaction, leading to inequality of bond lengths around the iron sites. The resulting dynamic problem has been solved for trimeric systems, but so far only in the d^1–d^1–d^0 and d^1–d^1–d^2 cases.[51] A full treatment for the present case of d^5–d^5–d^6 will be given elsewhere. Here it is sufficient to mention the results obtained in the limit of strong vibronic coupling, in which the electron transfer is introduced as a perturbation.[52] In the vibrational ground state ($n = 0$) the situation is the same as in Fig. 11. In the excited vibrational states, however, the resonance splitting is considerably larger by a factor of $[(\lambda^2/4\pi h\nu^3) - 1]$ where λ is the vibronic coupling parameter, so that $\lambda^2/4\pi h\nu^3$ is the number of vibrational quanta necessary for intervalence charge transfer. The relevant vibrational level is presumably around 760 cm^{-1}—our rough estimate of $\nu_{as}(Fe_3O)$—or less if other framework vibrations dominate the reorganisation process. Consequently, the electron delocalisation in the first vibrational state (n = 1) is even more pronounced than that described above for the exchange states at 100 and 130 cm^{-1}. These states become populated at higher temperatures, and on this basis the Mössbauer data are interpreted in terms of increasing contributions from static delocalisation, as distinct from lifetime broadening due to electron hopping.

The Mössbauer results for complex **2** in frozen THF solution, reported in this work, are different again. Only three

Table 8 DFT calculated energies and selected atomic charges of $[Fe_3OL_3]$, **2**

		Atomic charges in the Fe_3O core[b,c]			
Spin state	Total energy[a]	Fe^1	Fe^2	Fe^3	O
$S = 0$	−3740.522	+0.682	+0.686	+0.686	−0.609
$S = 1$	−3740.629	+0.759	+0.769	+0.769	−0.779
$S = 2$	−3740.643	+0.777	+0.760	+0.760	−0.767

[a] E(UB + HF − LYP) in Hartree units. [b] Mulliken atomic charges. [c] Compare an average value of 0.767, obtained for the iron centres in the monovalent cation ($S = 1/2$) with formal oxidation state +3.

doublets were required to fit the spectra, two of them consistent with partially localised valence states similar to those in the low-temperature component of the solid, *i.e.* Fe(2.85+, 2.85+, 2.3+), the other consistent with full delocalisation Fe(2.67+, 2.67+, 2.67+): $\delta = 0.66$ mm s^{-1} at 4.2 K and $\delta = 0.62$ mm s^{-1} at 160 K. The apparently delocalised component accounts for 70% of the molecules at 160 K. Again the data do not distinguish between static and dynamic situations.

In the oxo-centred carboxylate series, temperature-dependent Mössbauer spectra have been reported for many of the mixed-valence iron(III/II) complexes.[53,54] Only rarely have gradual transitions been observed. For example in the solid complex $[Fe_3O(OOCCH_3)_6(3\text{-Etpy})_3]\cdot CH_3CCl_3$, δ increases from 0.54 mm s^{-1} at 43 K to 0.60 mm s^{-1} at 100 K, and to 0.65 mm s^{-1} at 293 K, at which temperature the iron atoms are spectroscopically indistinguishable.[55] In most cases however, sudden transitions are observed from full valence localisation at low temperature, to spectra consistent with full delocalisation over three centres (or sometimes over only two centres, Fe(3+, 2.5+, 2.5+)) at higher temperature. The changes are then interpreted in terms of valence de-trapping, and absence of line broadening is explained by assuming that the internal electron transfer rate passes through the Mössbauer time scale rather rapidly, as the temperature is increased, in phase transitions controlled by cooperative effects in the solid state. In the present systems the outstanding feature of the Mössbauer data, in both solid and frozen solution states, is the evidence for some degree of valence delocalisation at the lowest temperatures.

Our discussion of ground and excited states is in reasonable agreement with the results of the DFT calculations. As shown in Table 8, the triplet and quintet states are significantly lower than the singlet, and this pattern qualitatively reflects the temperature-enhanced electron delocalisation discussed above. It is also of interest that the valence states appear more different in the triplet and quintet states than in the singlet state. The actual differences are small but the calculations were based on an almost symmetrical molecular model.

Conclusion

All indications are that the novel ligand system provides a rigid framework that substantially affects the electronic properties of the mixed-valence Fe_3O core. It also allows reversible formation of a series of one-electron redox states but still permits the fine-tuning of the electronic structure by environmental effects. In the solid state the mixing of valence states persists down to temperatures as low as 4.2 K, which has not been observed in any previous systems with this core structure. In both solid and solution states however, the valences of the three iron atoms remain inequivalent even up to room temperature. This means that at any instant in time, valence electron density is unequally distributed over the three atoms. The extent of this inequality, and whether it tends towards Fe(3+, 3+, 2+) or Fe(3+, 2.5+, 2.5+), are not specified, but in either case it is clear that the distribution rotates by an internal electron transfer process at a rate which is intermediate between the characteristic timescales of vibrational and Mössbauer spectroscopies. In terms of the Robin–Day classification, the mixed-valence iron complex is evidently at the borderline between classes II and III.

Acknowledgements

This work was supported by Deutsche Forschungsgemeinschaft and the Volkswagen-Stiftung. V. C. acknowledges the support of the Alexander von Humboldt Foundation, and T. I. the support of the Japan Society for the Promotion of Science. R. D. C. holds an Emeritus Leverhulme Fellowship.

References and notes

1 Recent reviews include: (*a*) C. C. Moser, C. C. Page, R. Farid and P. L. Dutton, *J. Bioenerg. Biomembr.*, 1995, **27**, 263; (*b*) P. F. Barbara, T. J. Meyer and M. A. Ratner, *J. Phys. Chem.*, 1996, **100**, 13148; (*c*) H. B. Gray and J. R. Winkler, *Annu. Rev. Biochem.*, 1996, **65**, 537; (*d*) H. B. Gray and J. R. Winkler, *Advances in Chemical Physics, Volume 106, Electron Transfer–From Isolated Molecules to Biomolecules, Part One*, ed. M. Bixon and J. Jortner, Wiley, New York, 1999, pp. 35–202.

2 (*a*) R. D. Cannon, *Electron Transfer Reactions*, Butterworth, London, 1980; (*b*) R. D. Cannon, *Electron Transfer in Inorganic, Organic and Biological Systems: (Adv. Chem. Ser., 228)*, ed. J. R. Bolton, N. Mataga and G. McLendon, ACS, Washington, DC, 1991; (*c*) A. M. Kuznetsov, *Charge Transfer Processes in Physics, Chemistry and Biology*, Gordon & Breach, New York, 1995.

3 (*a*) G. A. Neyhart, C. J. Timpson, W. D. Bates and T. J. Meyer, *J. Am. Chem. Soc.*, 1996, **118**, 3730; (*b*) T. Ito, T. Hamaguchi, H. Nagino, T. Yamaguchi, J. Washington and C. Kubiak, *Science*, 1997, **277**, 660; (*c*) K. D. Demadis, G. A. Neyhart, E. M. Kober and T. J. Meyer, *J. Am. Chem. Soc.*, 1998, **120**, 7121; (*d*) C. E. B. Evans, M. L. Naklicki, A. R. Rezvani, C. A. White, V. V. Kondratiev and R. J. Crutchley, *J. Am. Chem. Soc.*, 1998, **120**, 13096; (*e*) K. D. Demadis, E.-S. El-Samanody, G. M. Coia and T. J. Meyer, *J. Am. Chem. Soc.*, 1999, **121**, 535; (*f*) T. Ito, T. Hamaguchi, H. Nagino, T. Yamaguchi, H. Kido, I. S. Zavarine, T. Richmond, J. Washington and C. Kubiak, *J. Am. Chem. Soc.*, 1999, **121**, 4625; (*g*) C. Lambert and G. Nöll, *J. Am. Chem. Soc.*, 1999, **121**, 8434; (*h*) M. Ketterle, W. Kaim, J. A. Olabe, A. R. Parise and J. Fiedler, *Inorg. Chim. Acta*, 1999, **291**, 66.

4 R. D. Cannon and R. P. White, *Prog. Inorg. Chem.*, 1988, **36**, 195.

5 (*a*) S. J. Lippard, *Angew. Chem.*, 1988, **100**, 353; (*b*) S. J. Lippard, *Angew. Chem., Int. Ed. Engl.*, 1988, **27**, 344.

6 (*a*) T. Nakamoto, M. Hanaya, M. Katada, K. Endo, S. Kitagawa and H. Sano, *Inorg. Chem.*, 1997, **36**, 4347; (*b*) C.-C. Wu, S. A. Hunt, P. K. Gantzel, P. Guetlich and D. N. Hendrickson, *Inorg. Chem.*, 1997, **36**, 4717; (*c*) R. Wu, M. Poyraz, F. E. Sowrey, C. E. Anson, S. Wocadlo, A. K. Powell, U. A. Jayasooriya, R. D. Cannon, T. Nakamoto, M. Katada and H. Sano, *Inorg. Chem.*, 1998, **37**, 1913.

7 Y. Kaneko, M. Nakano, M. Sorai, H. G. Jang and D. N. Hendrickson, *Inorg. Chem.*, 1989, **28**, 1067 and references therein.

8 R. D. Cannon, U. A. Jayasooriya, S. K. Arap Koske, R. P. White and J. H. Williams, *J. Am. Chem. Soc.*, 1991, **113**, 4158.

9 R. Wu, S. K. Arap Koske, R. P. White, C. E. Anson, U. A. Jayasooriya and R. D. Cannon, *J. Chem. Soc., Chem. Commun.*, 1994, 1657.

10 (*a*) F. E. Sowrey, C. J. MacDonald and R. D. Cannon, *J. Chem. Soc., Faraday Trans.*, 1998, **94**, 1571; (*b*) F. E. Sowrey, Ph.D. Thesis, University of East Anglia, Norwich, 1997.

11 (*a*) R. Manchanda, *Inorg. Chim. Acta*, 1996, **245**, 91; (*b*) B. P. Straughan, O. M. Lam and A. Earnshaw, *J. Chem. Soc., Dalton Trans.*, 1987, 97; (*c*) G. Losada, M. A. Mendiola and M. T. Sevilla, *Inorg. Chim. Acta*, 1997, **255**, 125; (*d*) A. M. Bond, R. J. H. Clark, D. G. Humphrey, P. Panayiotopolous, B. W. Skelton and A. H. White, *J. Chem. Soc., Dalton Trans.*, 1998, 1845; (*e*) E. Constantinescu, H. Storch, C. Turta and V. Meriacre, *Rev. Roum. Chim.*, 1998, **43**, 799.

12 (*a*) R. W. Saalfrank, S. Trummer, H. Krautscheid, V. Schünemann, A. X. Trautwein, S. Hien, C. Stadler and J. Daub, *Angew. Chem.*, 1996, **108**, 2350; (*b*) R. W. Saalfrank, S. Trummer, H. Krautscheid, V. Schünemann, A. X. Trautwein, S. Hien, C. Stadler and J. Daub, *Angew. Chem., Int. Ed. Engl.*, 1996, **35**, 2206.

13 V. Coropceanu, V. Schünemann, C. Ober, M. Gerdan, A. X. Trautwein, J. Köhler and R. W. Saalfrank, *Inorg. Chim. Acta*, 2000, **300–302**, 875.

14 R. A. Henry and W. G. Finnegan, *J. Am. Chem. Soc.*, 1954, **76**, 923.

15 A. G. Oertli, W. R. Meyer, U. W. Suter, F. B. Joho, V. Gramlich and W. Petter, *Helv. Chim. Acta*, 1992, **75**, 184.
16 J. Salbeck, Ph.D. Thesis, Universität Regensburg, 1988, p. 196.
17 J. Salbeck, *Anal. Chem.*, 1993, **65**, 2169.
18 M. Büschel, C. Stadler, C. Lambert, M. Beck and J. Daub, *J. Electroanal. Chem.*, 2000, **484**, 24.
19 (*a*) A. D. Becke, *Phys. Rev. A*, 1988, **38**, 3098; (*b*) A. D. Becke, *J. Chem. Phys.*, 1993, **98**, 1372; (*c*) A. D. Becke, *J. Chem. Phys.*, 1993, **98**, 5648.
20 Gaussian-98, Revision A.7, M. J. Frisch, G. W. Trucks, H. B. Schlegel, G. E. Scuseria, M. A. Robb, J. R. Cheeseman, V. G. Zakrzewski, J. A. Montgomery, Jr., R. E. Stratmann, J. C. Burant, S. Dapprich, J. M. Millam, A. D. Daniels, K. N. Kudin, M. C. Strain, O. Farkas, J. Tomasi, V. Barone, M. Cossi, R. Cammi, B. Mennucci, C. Pomelli, C. Adamo, S. Clifford, J. Ochterski, G. A. Petersson, P. Y. Ayala, Q. Cui, K. Morokuma, D. K. Malick, A. D. Rabuck, K. Raghavachari, J. B. Foresman, J. Cioslowski, J. V. Ortiz, A. G. Baboul, B. B. Stefanov, G. Liu, A. Liashenko, P. Piskorz, I. Komaromi, R. Gomperts, R. L. Martin, D. J. Fox, T. Keith, M. A. Al-Laham, C. Y. Peng, A. Nanayakkara, C. Gonzalez, M. Challacombe, P. M. W. Gill, B. Johnson, W. Chen, M. W. Wong, J. L. Andres, C. Gonzalez, M. Head-Gordon, E. S. Replogle and J. A. Pople, Gaussian, Inc., Pittsburgh PA, 1998.
21 P. J. Hay and W. R. Wadt, *J. Chem. Phys.*, 1988, **82**, 299.
22 D. T. Cromer and J. T. Waber, in *International Tables for X-Ray Crystallography*, ed. J. A. Ibers and W. C. Hamilton, Kynoch Press, Birmingham, England, 1974.
23 G. M. Sheldrick, *Acta Crystallogr., Sect. A*, 1990, **46**, 467.
24 (*a*) G. M. Sheldrick, SHELXL-93, Program for refinement of crystal structures, University of Göttingen, 1993; (*b*) SHELXL-93: G. M. Sheldrick, in *Crystallographic Computing 3*, ed. G. M. Sheldrick, C. Krüger and R. Goddard, Oxford University, 1993, pp. 175–189; (*c*) SHELXL-97: G. M. Sheldrick, University of Göttingen, 1997.
25 Crystal structure determinations were carried out by Frank Hampel (Erlangen) and by Regine Herbst-Irmer and Cornelia Goebel, (Institut für Anorganische Chemie, Universität Göttingen, Tammanstrasse 4, D-37077, Göttingen, Germany).
26 H. G. Jang, K. Kaji, M. Sorai, R. J. Wittebort, S. J. Geib, A. L. Rheingold and D. N. Hendrickson, *Inorg. Chem.*, 1990, **29**, 3547.
27 (*a*) K. Nakamoto, *Infrared and Raman Spectra of Inorganic and Coordination Compounds*, 4th edn., John Wiley, New York, 1986; (*b*) V. Galasso, G. de Alti and G. Costa, *Spectrochim. Acta*, 1965, **21**, 660.
28 D. A. Long and E. L. Thomas, *Trans. Faraday Soc.*, 1963, **59**, 783.
29 T. Miyazawa, T. Shimanouchi and S.-I. Mizushima, *J. Chem. Phys.*, 1958, **29**, 611.
30 A. Bigotto and R. Klingendrath, *Spectrochim. Acta, Part A*, 1990, **46**, 1683.
31 P. Carmona, *Spectrochim. Acta, Part A*, 1980, **36**, 705.
32 The following is a list of differences in standard reduction potential of the two isostructural couples, $\Delta E = E(\mathrm{Co^{III/II}}) - E(\mathrm{Fe^{III/II}})$, measured in the same medium at the same temperature—usually 293–298 K. Each consists of the formula of the complex, ML_n (M = Co, Fe), the value of ΔE in V, and the literature reference. $[M(OH_2)_6]^{3+/2}$, 1.13,[33] $[M(C_2O_4)_3]^{3-/4}$, 0.56;[33] $[M(acac)_3]^{0/-}$, 0.29;[34] $[M(edta)]^{-/2-}$, 0.28,[35] (Fe),[36] (Co); $[Fe^{III}{}_2MOL_3]^{0/-}$, −0.05, this work; $[CH_2(CH_2NCHC_6H_4O\text{-}o)_2M]^{+/0b}$, −0.20;[37] $[M(phen)_3]^{3+/2+}$, −0.73;[33] $[M(C_5H_5)_2]^{+/0}$, −1.30;[37] $[M(C_5Me_5)_2]^{+/0}$, −1.43.[38]
33 *Standard Potentials in Aqueous Solution*, ed. A. J. Bard, R. Parsons and J. Jordan, IUPAC, Marcel Dekker, New York, 1985.
34 O. Sock, P. Lemoine and M. Gross, *Electrochim. Acta*, 1981, **26**, 99.
35 N. Tanaka, T. Tomita and A. Yamada, *Bull. Chem. Soc. Jpn.*, 1970, **43**, 2042.
36 G. Schwarzenbach and J. Heller, *Helv. Chim. Acta*, 1951, **34**, 576.
37 K. J. Vetter and N. Jäger, *Electrochim. Acta*, 1966, **11**, 401.
38 (*a*) U. Koelle and F. Khouzami, *Angew. Chem.*, 1980, **92**, 658; (*b*) U. Koelle and F. Khouzami, *Angew. Chem., Int. Ed. Engl.*, 1980, **19**, 640.
39 R. P. White, L. M. Wilson, D. J. Williamson, G. R. Moore, U. A. Jayasooriya and R. D. Cannon, *Spectrochim. Acta, Part A*, 1990, **46**, 917.
40 P. Gütlich, R. Link and A. X. Trautwein, *Mössbauer Spectroscopy and Transition Metal Chemistry*, Springer-Verlag, Berlin, 1978.
41 C.-C. Wu, H. G. Jang, A. L. Rheingold, P. Gütlich and D. N. Hendrickson, *Inorg. Chem.*, 1996, **35**, 4137.
42 A. B. Edwards, J. M. Charnock, C. D. Garner and A. B. Blake, *J. Chem. Soc., Dalton Trans.*, 1995, 2515.
43 R. D. Cannon, U. A. Jayasooriya, R. P. White and S. K. Arap Koske, *Spectrochim. Acta, Part A*, 1993, **49**, 1787.
44 (*a*) L. Meesuk, U. A. Jayasooriya and R. D. Cannon, *J. Am. Chem. Soc.*, 1987, **109**, 2009; (*b*) R. W. Wu, U. A. Jayasooriya and R. D. Cannon, *Spectrochim. Acta, Part A*, 2000, **56**, 575.
45 R. P. White, Ph.D. Thesis, University of East Anglia, Norwich, 1991, p. 126.
46 For example a μ-oxo-bridged diiron(III,II) complex has been characterised as valence-localised, even though K_{com} is similar to the values reported here: A. S. Borovik, V. Papaefthymiou, L. F. Taylor, O. P. Anderson and L. Que, Jr., *J. Am. Chem. Soc.*, 1989, **111**, 6183.
47 (*a*) N. S. Hush, *Prog. Inorg. Chem.*, 1967, **8**, 391; (*b*) N. S. Hush, *Coord. Chem. Rev.*, 1985, **64**, 135.
48 M. B. Robin and P. Day, *Adv. Inorg. Chem. Radiochem.*, 1967, **30**, 247.
49 For $\delta[Fe^{3+}]$ we used the average of the values observed for the mixed-metal complexes $[Fe_2MOL_3]$ and the fully oxidised $[Fe_3OL_3]^+$, *i.e.* 0.46 mm s^{-1}, and for $\delta[Fe^{2+}]$ the typical[50] value 1.1 mm s^{-1}.
50 D. P. E. Dickson and F. J. Berry, *Mössbauer Spectroscopy*, Cambridge University Press, Cambridge, 1968, p. 88.
51 S. I. Boldyrev, V. Y. Gamurar, B. S. Tsukerblat and A. V. Palii, *Mol. Phys.*, 1994, **81**, 621.
52 R. L. Fulton and M. Gouterman, *J. Chem. Phys.*, 1961, **35**, 1059.
53 (*a*) S. M. Oh, D. N. Hendrickson, K. L. Hassett and R. E. David, *J. Am. Chem. Soc.*, 1984, **106**, 7984; (*b*) S. M. Oh, T. Kambara, D. N. Hendrickson, M. Sorai, K. Kaji, S. E. Woehler and R. J. Wittebort, *J. Am. Chem. Soc.*, 1985, **107**, 5540; (*c*) T. Kambara, D. N. Hendrickson, M. Sorai and S. M. Oh, *J. Chem. Phys.*, 1986, **85**, 2895; (*d*) M. Sorai, Y. Shiomi and D. N. Hendrickson, *Inorg. Chem.*, 1987, **26**, 223; (*e*) J. K. McCusker, H. G. Jang, M. Zvagulis, W. Ley, H. Drickamer and D. N. Hendrickson, *Inorg. Chem.*, 1991, **30**, 1985.
54 (*a*) T. Nakamoto, M. Katada and H. Sano, *Chem. Lett.*, 1990, 225; (*b*) T. Nakamoto, M. Katada and H. Sano, *Chem. Lett.*, 1991, 1323; (*c*) T. Nakamoto, M. Katada and H. Sano, *Hyperfine Interact.*, 1991, **68**, 233; (*d*) M. Yoshida, T. Nakamoto, S. Kawata, M. Katada and H. Sano, *Hyperfine Interact.*, 1994, **84**, 583; (*e*) M. Yoshida, T. Nakamoto, S. Kawata, M. Katada and H. Sano, *Hyperfine Interact.*, 1994, **84**, 589; (*f*) T. Nakamoto, M. Katada, S. Kawata, S. Kitagawa, H. Sano and M. Konno, *Hyperfine Interact.*, 1994, **93**, 1567; (*g*) T. Sato, A. Fumitoshi, K. Endo, M. Katada, T. Nakamoto and H. Sano, *J. Am. Chem. Soc.*, 1996, **118**, 3450; (*h*) T. Nakamoto, M. Katada and H. Sano, *Inorg. Chim. Acta*, 1999, **291**, 127.
55 G. Wu, Y. Zhang, L. Ribaud, P. Coppens, C. Wilson, B. B. Iversen and F. K. Larsen, *Inorg. Chem.*, 1998, **37**, 6078.